

Thermometry and Detector Electronics for the Cosmology Large  
Angle Sky Surveyor (CLASS) High Frequency Cryogenic Receiver

Manwei Chan

December 2015

# Contents

<b>1 Abstract</b>	<b>4</b>
<b>2 Acknowledgements</b>	<b>5</b>
<b>3 Introduction to the <math>\Lambda</math>CDM Model</b>	<b>6</b>
3.1 Overview . . . . .	6
3.2 Problems with the $\Lambda$ CDM Model . . . . .	8
3.2.1 The Flatness Problem . . . . .	8
3.3 The Horizon Problem . . . . .	10
3.4 The Monopole Problem . . . . .	10
3.5 The Inflation Solution . . . . .	10
<b>4 Inflation and the CMB</b>	<b>11</b>
4.1 Thompson Scattering and Polarization . . . . .	11
4.2 B-mode Foregrounds . . . . .	13
<b>5 CLASS: Cosmology Large Angular Scale Surveyor</b>	<b>14</b>
5.1 Experimental Strategy . . . . .	14
5.2 VPM . . . . .	16
5.3 Cryostat . . . . .	18
5.3.1 Overall Design . . . . .	19
5.3.2 Pulse Tube . . . . .	21
5.3.3 Dilution Refrigerator . . . . .	21
5.3.4 Thermometry . . . . .	22
5.3.5 Detectors . . . . .	23
<b>6 Conclusion</b>	<b>28</b>
<b>Appendices</b>	<b>29</b>
<b>Appendix A The Cosmological Equations</b>	<b>29</b>
<b>Appendix B TekData Cables</b>	<b>30</b>

<b>Appendix C Cryostat Operating Procedures</b>	<b>31</b>
C.1 These are activities that should only have to be done once . . . . .	31
C.2 These are activities that should be checked every time the cryostats are closed . . . . .	32
<b>Appendix D Site Work</b>	<b>33</b>
D.1 Acquiring Data . . . . .	33

# 1 Abstract

The theory of inflation is a widely accepted, but unproven theory. It postulates the rapid expansion of the universe when it was  $10^{-36}$  seconds old. This rapid expansion would have created gravitational waves which would leave an imprint on the Cosmic Microwave Background by producing B-mode polarization. The Cosmology Large Angular Scale Surveyor endeavors to measure this B-mode polarization spectrum with a sensitivity of  $r = 0.01$ . Detection of this signal requires highly sensitive equipment that will be housed in cryostats. My project has been to prepare one of these cryostats for deployment in the field.

## 2 Acknowledgements

I would like to thank everyone who made my work with CLASS enjoyable, fruitful, and fun. I would like to thank Professor Tobias Marriage, who welcomed me into his lab the summer after my freshman year and has acted as a mentor throughout my undergraduate career. I would also like to thank Jeff Iuliano, with whom I worked very closely to prepare the cryostat. I thank the post docs Lucas Parker, John Appel, Joseph Eimer, and Tom Essinger-Hileman for guiding me through my work and answering all my questions. I am indebted to Zhilei Xu for his friendship, mentorship, and giving me a mug from which I drink his tea. I would like to thank Katie, Sumit, and Devin for answering the questions I didn't want to bother the post docs with. Thanks to my office mate and friend since I arrived at Johns Hopkins University, Nick Merhle. Lastly, I would like to thank the rest of the CLASS collaboration and anyone else who has helped me along the way. I am forever grateful to be apart of this lab for it has given me more than I can ever acknowledge.

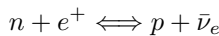
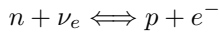
### 3 Introduction to the $\Lambda$ CDM Model

#### 3.1 Overview

The  $\Lambda$  Cold Dark Matter ( $\Lambda$ CDM) model for cosmology is known as the standard model for cosmology because it is the most accurate theory we have for describing observable phenomena. It is a Big Bang model that incorporates dark energy, the driving force behind the expansion of our universe described by the cosmological parameter  $\Lambda$ , and cold dark matter, a type of matter that only interacts through the gravitational force.<sup>1</sup> In particular, dark matter does not interact with electromagnetic waves and is thus generally difficult to detect.

The model begins with the Big Bang event, which was actually not an explosion. During the Big Bang, the observable universe began as an infinitesimally small and dense space-time object which then expanded. In the very beginning, the temperature of the universe was too hot for matter to stick together, even quarks could not combine to form protons and neutrons. As the universe grew, the temperature dropped, allowing matter to combine in a stable manner.

The first observable predicted by the  $\Lambda$ CDM model is the relative abundances of the light elements, created in the process of Big Bang Nucleosynthesis (BBN). Around 0.1 seconds after the beginning of the universe, after quarks combined to form neutrons and protons, these baryons were in equilibrium through the interactions:



Since these interactions are mediated by neutrinos, and therefore the weak force, protons and neutrons ceased being in equilibrium once the temperature dropped enough, roughly when the age of the universe was 1 second old<sup>2</sup>. At around  $t = 200$  s protons and neutrons combine to start forming deuterium. Once enough deuterium forms, other fusion reactions were possible creating  $^3\text{He}$ ,  $^4\text{He}$ , and trace amounts of  $^6\text{Li}$  and  $^7\text{Li}$ . BBN was a race against time because as the universe expanded these fusion reactions were no longer possible at cooler temperatures. By taking into account various parameters such as the relative abundances

---

<sup>1</sup>This particular type of dark matter is labeled cold because it is traveling at non-relativistic speeds (speeds much slower than the speed of light). It is needed to explain phenomena such as the rotational curves of galaxies and galaxy cluster clumping behavior. Hot dark matter, such as neutrinos, would be traveling too fast to stay localized in galaxies and galaxy clusters.

<sup>2</sup>The cross-sections for weak interactions have a temperature dependence of  $\sigma \propto T^2$ , so as the temperature drops, neutrinos stop interacting with protons and neutrons, bringing them out of equilibrium.

of protons and neutrons at the beginning of BBN and the decay rate of the neutrons, the relative abundances of these light elements can be predicted and observed today.

Another observable predicted by the  $\Lambda$ CDM Big Bang Model is the Cosmic Microwave Background (CMB). At one point, the universe was hot enough that all the hydrogen (protons left over from BBN), and other nuclei created during BBN were ionized because photons were energetic and abundant enough to dislodge any electrons that could be captured by the nuclei. Since photons were constantly interacting and being deflected in different directions, the universe was effectively opaque to light. However, at about 380,000 years after the beginning of the universe, the temperature cooled enough for nuclei to capture electrons. Photons no longer had the energy to force out electrons from nuclear orbits and after the epoch of last scattering, could travel unimpeded through the universe. This light can be seen today as a glow in the microwave wavelength at every point in the sky and has been coined the CMB.

Evidence of the need to include dark matter in our model can be found in small temperature fluctuations of the CMB. At larger angular scales ( $\theta > 1^\circ$ ), the fluctuations are caused by the Sachs-Wolfe effect. At the time of last scattering, the distribution of dark matter was not uniform, creating a gravitational potential landscape. At a minima in the potential (potential well), a photon would have to 'climb' out of this well at last scattering, lose energy in the process and be relatively more redshifted than a photon that was at a maxima (potential hill), which would gain energy when escaping the hill. At angular scales of  $\theta < 1^\circ$ , the cause of the fluctuations are dominated by a different effect. Before last scattering, the photons, electrons, and protons were coupled and behaved together as a photon-baryon fluid. Dark matter behaved independently of this fluid, and as the fluid fell into potential wells, the fluid would be compressed, increasing the pressure and causing it to expand outward until the pressure dropped enough for gravity to cause the fluid to fall inward again. This process continued until last scattering and is named baryonic acoustic oscillations. At last scattering, if the photon was part of a compressed fluid, it would be released with a higher energy than a photon that was a part of an expanded fluid. Measurements of these temperature fluctuations confirmed that dark matter is needed to explain these properties of the CMB. Additionally, observations from galaxy cluster escape velocities[22], gravitational lensing, and velocity rotation curves of galaxies[15] all imply the existence of dark matter. Lastly, the fluctuations are indicative of the non-homogeneity of the early universe. The slightly denser regions of dark matter will attract more matter through gravity, eventually leading to the large scale distribution of galaxies, clusters, etc. in our universe today. The necessity for dark matter in the evolution of the universe is included in the  $\Lambda$ CDM model. A more detailed description of BBN and the CMB can be found in Ryden's Introduction to Cosmology[17].

The last observable our model must include is  $\Lambda$ . Observations of Type Ia supernovae, the amount of gravitational lensing along a line of sight, the number of rich galaxy clusters<sup>3</sup>, and other cosmological observables show that the universe is expanding at an accelerating rate[14][3]. To account for this rate, the introduction of dark energy had to be introduced into the model as well.

## 3.2 Problems with the $\Lambda$ CDM Model

Even though the  $\Lambda$ CDM Model agrees with current observable phenomena, it still fails to explain three major problems, which will be detailed below.

### 3.2.1 The Flatness Problem

Einstein's Theory of General Relativity provides the equations to describe the curvature of space-time. Within the context of general relativity, Alexander Friedmann developed equations to describe the expansion of space. Within these equations, the curvature of space-time is related to the energy density parameter  $\Omega$ , which is the ratio of the actual energy density to the critical energy density.

$$\Omega(t) = \frac{\epsilon(t)}{\epsilon_c(t)}$$

The energy density is determined by the amount of matter (visible and dark) and dark energy in the universe. See Appendix A for a more in-depth discussion of the cosmological equations. If  $\Omega > 1$ , the universe is positively curved. An example of a positively curved space which can be intuitively grasped is the surface of a sphere. This is a 2 dimensional space where the interior angles of any triangle drawn on the surface will have a sum of more than  $180^\circ$ . Conversely, a negatively curved universe, which will have  $\Omega < 1$ , would look like a saddle in 2 dimensional space where the interior angles of a triangle will have a sum of less than  $180^\circ$ . Lastly, if the energy density is equal to the critical energy density,  $\Omega = 1$ , which would look like flat euclidean space where the interior angles of a triangle will have a sum of exactly  $180^\circ$ . See Figure 1 for an illustration of curvature in 2 dimensional space.

The curvature of space time is also related to the fate of our universe. In a positively curved universe, the force of gravity overcomes the expansionary force of dark energy and the universe ends in a Big Crunch, where everything collapses back into a singularity. The flat and negatively curved universes share similar fates, which is either the Big Freeze or the Big Rip. In the Big Freeze, the universe continues

---

<sup>3</sup>Rich galaxy clusters are filled with hundreds to thousands of galaxies as opposed to poor galaxy clusters which only have a few galaxies.

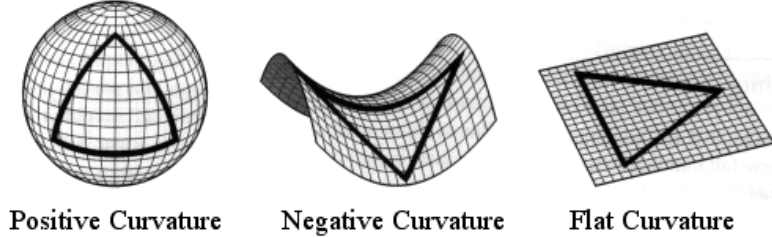


Figure 1: A depiction of curvature in 2 dimensional space, which may help with the intuitive understanding of spatial curvature. Figure from [1]

to expand until the temperature of the universe asymptotically reaches absolute zero. In the Big Rip, the expansionary force continually increases to the point where all material objects in the universe will eventually be ripped apart into elementary particles and radiation.

An interesting point to note is that if we include dark energy into our model, we could also have a flat universe that results in a Big Rip since the dark energy drives exponential expansion. This can be explained through the equation of state parameter  $w$ . The density of the components of the universe scale as

$$\rho = a^{-3-3w}$$

where  $\rho$  is the density and  $a$  is the scale factor (see Appendix A). For ordinary (non-relativistic) matter,  $w = 0$  so the density scales as  $\rho = a^{-3}$ , which makes sense since matter density is inversely proportional to volume. For radiation,  $w = 1/3$  so  $\rho = a^{-4}$  because as the universe expands, radiation is also red-shifted, adding another factor of energy density dilution in addition to dilution through volume expansion. The equation of state of dark energy hasn't been accurately measured yet, but is believed to be around  $w = -1$ . In the case that  $w < -1$  then the density of dark energy increases as the universe expands (since the exponent in the density equation is  $> 1$ ), accelerating the expansion of our universe and ultimately ending in the Big Rip.

Recent observations from experiments such as WMAP have shown that the curvature of our universe is very close to flat. In fact, during the time of nucleosynthesis, the density of the universe differed from the critical density by one part in 30 trillion. If that difference had been only one part in 30 thousand, the universe would have met its fate in the Big Crunch or the Big Chill after only a few years[17]. This fine-tuning of the energy density, and therefore the curvature of the universe, calls into question why these parameters exist in such a way that allows humans to exist. This question is considered the flatness problem

as the  $\Lambda$ CDM Model provides no mechanism to explain why our universe is flat [10].

### 3.3 The Horizon Problem

The horizon problem questions the homogeneity and isotropy of our universe. Imagine two antipodal points on the CMB,  $180^\circ$  apart. Let's say one of these points, point A, is directly above Earth's north pole and the other, point B, is located directly below Earth's south pole. The time it takes for light from point A to reach the Earth is almost the age of the universe. For light from point A to reach point B would take a time almost twice the age of the universe, and since information cannot travel faster than the speed of light, these two points cannot be causally connected. In other words, these two points could not have exchanged information, meaning they have no reason to be related at all. Nevertheless, the entire CMB, including points A and B, have the same temperature in one part in  $10^5$ . This brings forward the question of how the CMB can be so uniform if points were never in thermal contact with one another. In fact, points separated by a mere  $2^\circ$  on the CMB should not be causally related. There are 20,000 patches of the CMB that are all non causally related to one another, yet they all share pretty much the same temperature. The  $\Lambda$ CDM Model again provides no mechanism to explain this uniformity [17].

### 3.4 The Monopole Problem

Theorists predict that on high enough energy scales, the strong, weak, and electromagnetic forces are unified under one force. This Grand Unified Theory is valid at energies supported during the Big Bang, but as the universe cooled to  $10^{28}$  K, there was a phase transition when the force separated into the strong force and the electroweak (electromagnetic and weak force were still unified) force. This phase transition should give rise to topological defects, one of which is the existence of a magnetic monopole. A magnetic monopole is the existence of either the north or south pole of a magnet without the existence of the other.<sup>4</sup> We have never detected a magnetic monopole [17].

### 3.5 The Inflation Solution

In 1981, Alan Guth proposed a solution to the problems detailed above. He proposed that the universe expanded exponentially when it was around  $10^{-36}$  seconds old. Inflation would solve the flatness problem because the expansion would have flattened the universe. Even if the universe began strongly curved, a strong inflationary period would have flattened the universe to a flatness we observe today. The

---

<sup>4</sup>An electron is an example of an electric monopole.

horizon problem is solved since inflation allows the visible universe to be in thermal contact before inflation. It is only after inflation expands space time exponentially that there are parts of the visible universe that are not causally connected anymore, which explains why the CMB is relatively homogeneous. Lastly, assuming that the creation of magnetic monopoles happened before or during inflation, the number density of the monopoles would be diluted to the point where the probability of finding one within the visible universe today would be astronomically small [17].

## 4 Inflation and the CMB

There have been many observations, like the ones mentioned above, that support the theory of inflation. However, to date the most compelling evidence for inflation would be to detect primordial B-mode polarization patterns on the CMB since the explosive expansion of the universe would have left an imprint on the CMB itself.

### 4.1 Thompson Scattering and Polarization

CMB photons are polarized from Thompson Scattering. Thompson Scattering occurs when the electric field of an incoming photon accelerates a charged particle (in our case a free electron), which in turn emits another photon at the same frequency. While each emitted photon has a definite polarization state, in an isotropic radiation field, the emitted radiation (sum of all emitted photons) from Thompson Scattering will have no net polarization. In order to get emitted radiation with a net linear polarization, the intensity of the incoming radiation must vary by 90 degrees, creating a quadrupole pattern. For example take radiation coming in from the x-axis (polarization states along z and y axes), which is then scattered along the z-axis. The emitted radiation only retains one of the incoming polarization states, the one along the y-axis, since light cannot be polarized in its direction of motion (z-axis). By introducing radiation coming in from the y-axis with different intensity than the radiation coming in from the x-axis, the emitted radiation will now have a net linear polarization. See Figure 2 for an illustration.

As seen in the figure, this scenario occurs due to a quadrupole anisotropy existing around the free electron. There are three forms of perturbations of space-time, also called metric perturbations that give rise to quadrupole anisotropies: scalar, vector, and tensor.<sup>5</sup> Scalar anisotropies are caused by density

---

<sup>5</sup>These can be thought of in terms of the multipole decomposition of the radiation field into spherical harmonics. A Quadrupole anisotropy is represented by  $l = 2$  (dipole would be  $l = 1$  and monopole  $l = 0$ ), while the scalar, vector, and tensor moments are represented by  $m = \pm 1$ ,  $m = \pm 2$ , and  $m = \pm 3$  respectively.

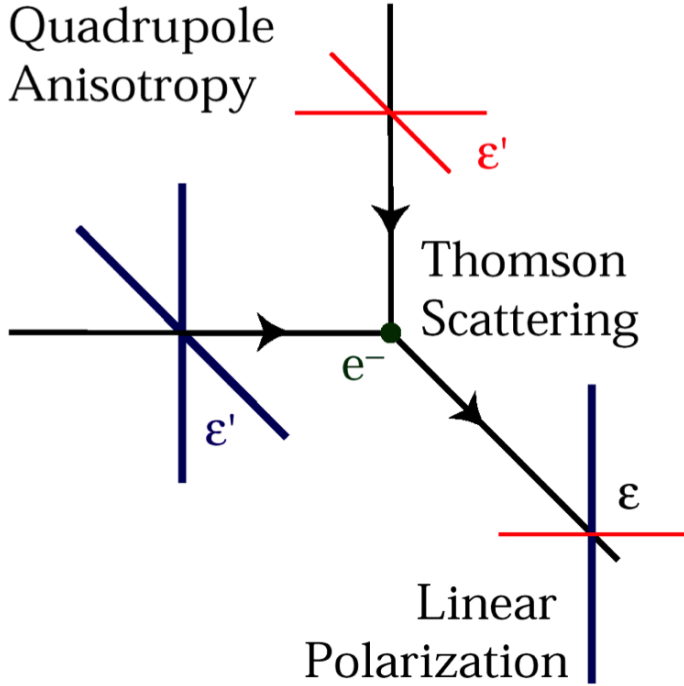


Figure 2: In the illustration radiation with higher intensity (blue) is incident on a free electron along the horizontal axis and less intensity radiation (red) is incident along the vertical axis. The free electron will then emit net polarized radiation along the axis coming out of the page [6].

fluctuations, which formed because quantum fluctuations provide a non-homogeneous distribution of matter. Vector perturbations are caused by the vortical motion of matter. An observer located between two layers of matter moving in opposite directions will experience a vector perturbation due to the Doppler effect. However, vorticity is expected to be dampened by inflation to the point where it becomes negligible to polarization. The last type, tensor perturbation, are gravitational waves. Heuristically, gravity waves stretch and squeeze the space around the free electron in such a way that it creates the tensor anisotropy [11].

The polarization pattern can be separated into its “electric” (E) and “magnetic” (B) components. The decomposition of the CMB is crucial to determining if inflation occurred. See Figure 3 for an illustration. E-modes can be created by scalar and tensor perturbations, while B-modes can be created by tensor perturbations, thus gravitational waves are the only generators of B-modes in the CMB. Because inflation and the explosive expansion of the universe during that epoch were predicted to create gravitational waves, detecting these primordial B-modes would provide evidence that inflation occurred. Also, inflation would stretch quantum fluctuations in space-time to universe-sized gravitational waves, and observing these primordial B-modes would also be proof of quantum gravity.

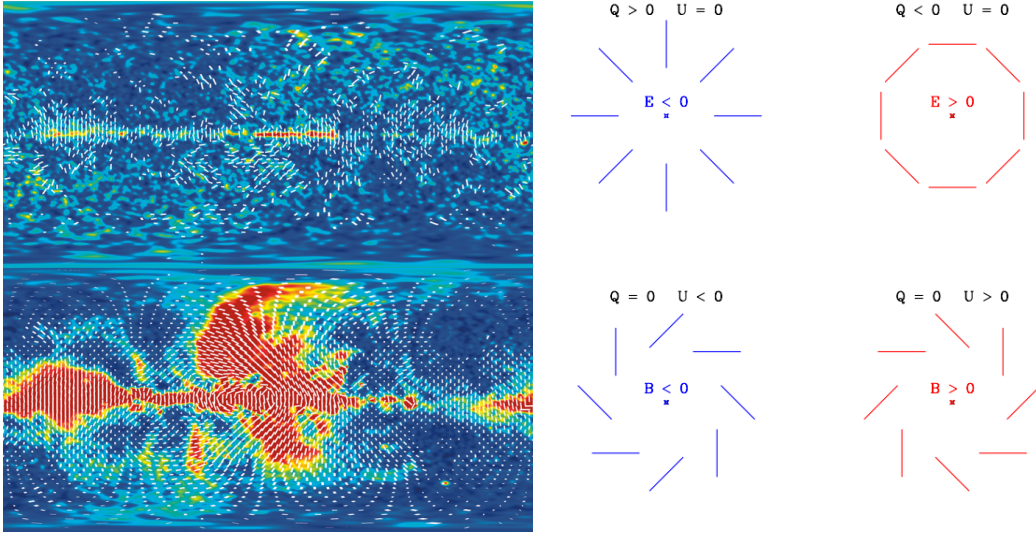


Figure 3: The images on the left are polarization maps of the CMB from WMAP [20]. The image on the top is taken at 23 GHz and the image on the bottom is taken at 94 GHz. These polarization patterns can then be decomposed into the E and B-modes seen on the right [21]. Notice how the E-modes remain unchanged if reflected while the B-modes will seem to curl in the other direction if reflected.

## 4.2 B-mode Foregrounds

Unfortunately, observing primordial B-modes produced by inflation is not an easy task. There are multiple foreground phenomena that obscure the primordial polarization signal. The three primary foregrounds are synchrotron radiation, free-free radiation, and dust. At lower frequencies (20-40 GHz), the polarization foreground is dominated by synchrotron and free-free radiation. Synchrotron is the most pervasive and is created by relativistic electrons accelerated in strong magnetic fields, which in turn radiate polarized photons. Free-free emission, also known as Bremsstrahlung, is caused by the acceleration of an electron when it comes into proximity of another charged particle, and this acceleration causes the electron to emit a photon. While free-free radiation is intrinsically unpolarized, it can be partially polarized by Thompson scattering within the HII region, a region of partially ionized gas where star formation has recently taken place. However, this effect is small and is not expected dominate the polarization at any frequency. At higher frequencies ( $>80$  GHz), polarized emission from dust particles becomes the dominant foreground. Interstellar dust comes in asymmetric shapes, but magnetic fields tend to align the longer axis of these grains at right angles to the direction of the field. A dust grain is more likely to scatter a photon if the photon's electric field is parallel to the long axis of the grain; therefore, light with no net polarization that enters a dust cloud where the particles are aligned will come out with a net polarization. A map of the dust foreground can be seen in Figure 4. Accounting for the low frequency synchrotron and high frequency

dust foregrounds, the minimum in foreground occurs around 100 GHz [11].

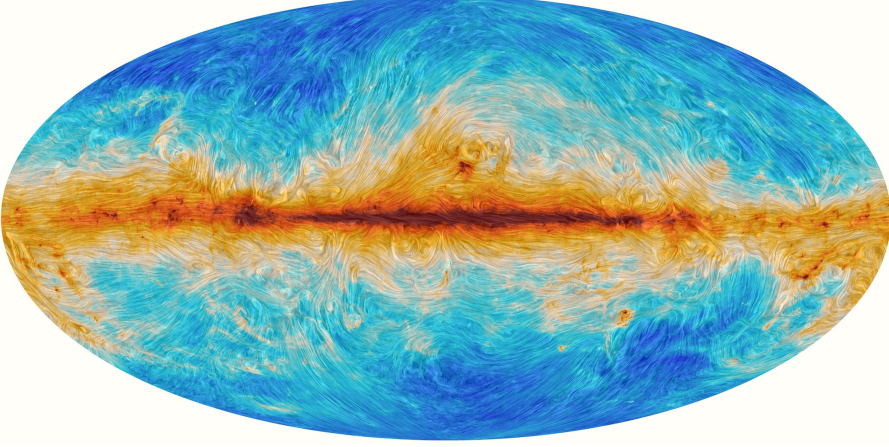


Figure 4: A map of the polarized emission from Milky Way Dust from the Planck Collaboration. The colors indicate the intensity of dust emission with red being stronger and blue weaker [13].

## 5 CLASS: Cosmology Large Angular Scale Surveyor

### 5.1 Experimental Strategy

The Cosmology Large Angular Scale Surveyor (CLASS) is an experiment measuring the imprint from inflation on the CMB. The telescope will operate at an altitude of 5200 meters (17,100 feet) from Cerro Toco in the Atacama desert. The Atacama desert is dry and at a high altitude, limiting atmospheric interference. It will be located at a latitude of approximately  $-23^\circ$ , as opposed to other ground based telescopes observing the CMB, which are located at the South Pole. This allows CLASS to observe 70% of the sky, allowing the experiment to investigate the properties of the CMB at larger angular scales, the importance of which are detailed in Figure 5 [8].

CLASS will also operate in four frequency bands centered at 38, 93, 148, and 217 GHz. For ease of using round numbers we will call them the 40, 90, 150, and 220 GHz bands, respectively. CLASS bands are associated with different telescopes. One operates at 40 GHz; two operate at 90 GHz, and the last will operate at 150 and 220 GHz. This layout can be seen in Figure 6. These bands were specifically chosen to avoid the prominent oxygen and water emission lines in the atmosphere. Multiple bands are used in order to give the experiment a chance to subtract the polarization foregrounds detailed above. The 40 GHz band will measure the synchrotron foreground, while the 220 GHz bands will measure the foreground due to dust.

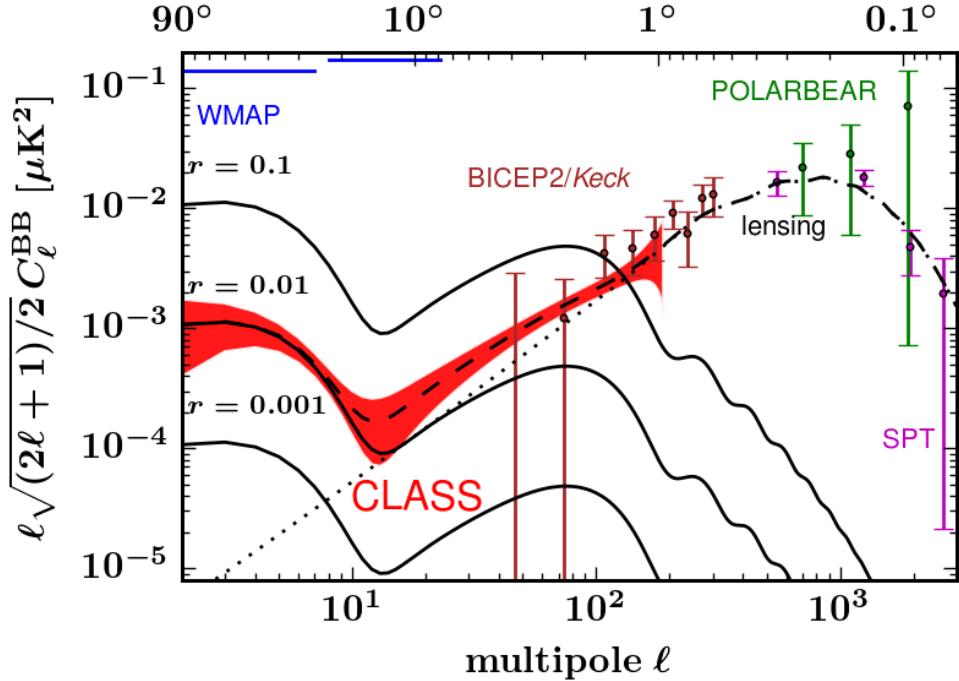


Figure 5: The first thing to note in the figure are the spectra labeled with an  $r$  value.  $r$  is the tensor-to-scalar ratio, which measures the amplitude of the tensor anisotropies, and therefore the energy scale of inflation. The lower  $r$  is, the more sensitive instruments have to be. Each line represents the B mode spectrum at each value of  $r$ . When we decompose the polarization of the CMB into E and B modes, we decompose the sky through spherical harmonics, and the  $l$  values corresponding to each spherical harmonic are located along the x-axis. Another way to think of the decomposition is that higher  $l$  values correspond to smaller angular scales and lower  $l$  values to larger angular scales. The dotted line is the B mode spectrum caused by gravitational lensing. Large scale structures can turn primordial E modes into B modes through lensing. Note that gravitational lensing dominates at smaller angular scales, so in order to detect the primordial B mode spectrum we have to look at larger angular scales. Note how many of the other experiments (WMAP) did not have the sensitivity to probe low  $r$  values, while others (BICEP2, POLARBEAR, etc.) are not able to investigate lower  $l$  values. What makes CLASS unique (shaded in red) is its ability to probe both large angular scales at a sensitivity that can measure or place an upper limit at  $r = 0.01$ .

The 90 GHz and 150 GHz detectors will be the main science bands that will be used for CMB analysis. Additionally, to help control systematic errors and improve the sensitivity of measurements, CLASS will utilize a fast polarization modulation using a variable-delay polarization modulator (VPM) and cryogenic housing, both of which will be detailed below.

## 5.2 VPM

CLASS will use fast polarization modulation in order to separate the sky polarization from polarization created by the instrument itself, reduce  $1/f$  noise from unpolarized atmospheric emissions, and also provide a measurement of circular polarization. The VPM consists of a flat movable mirror behind a stationary wire grid. The wire grid is made of 3900 copper-plated tungsten wires with a diameter of  $50.8 \mu m$  all placed parallel to one another with a spacing of  $159.5 \mu m$  between them. The mirror will modulate at a frequency of 10 Hz with an amplitude of approximately 1.5 mm (peak-to-peak distance of 3 mm) for the 40 GHz receiver [12].

Incident light is separated into two orthogonal linear polarization states by the wire grid. Light polarized parallel to the direction of the wires is reflected while light polarized orthogonal to the wires is transmitted. The transmitted light reflects off the mirror and passes back through the grid to recombine with the signal that was reflected by the grid, except now with a different phase offset than the incident light. By modulating the distance between the grid and the mirror, incoming polarization patterns can be modulated from linear to circular and from circular to linear. A schematic of this can be seen in Figure 7.

Because the VPM is the first element of the telescope incident light hits when entering the telescope system, it can help determine how much of the detected polarization is created by mirrors and other optical properties of the instrument itself. Because the VPM only modulates the celestial polarization, the polarization from the sky and from the instruments can be differentiated. Additionally, since the VPM modulates polarized light, it is also useful in differentiating the polarized celestial signal from unpolarized signals. It acts like a lock-in amplifier modulating the signal at 10 Hz. This helps reduce  $1/f$  noise which is dominant at under 1 Hz. By applying techniques such as filters and Fourier transforms, we can study the signal at 10 Hz where  $1/f$  noise is greatly reduced. Lastly, as stated before, linearly polarized light can be converted to circularly polarized light. However, it is expected there should be no circularly polarized light from the sky, so our expected null measurements of circularly polarized light will help scientists understand the systematic errors associated with CLASS [7].

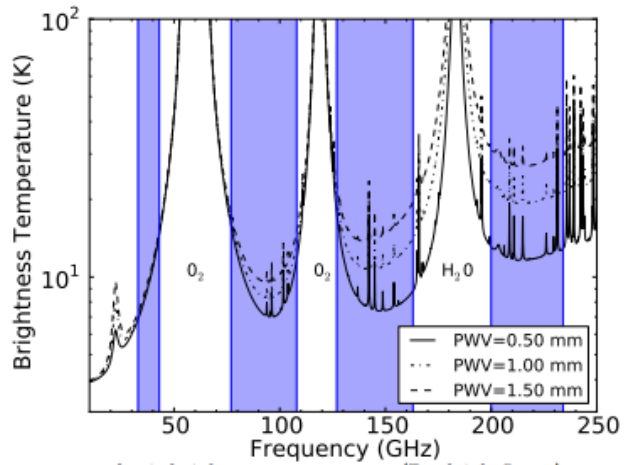
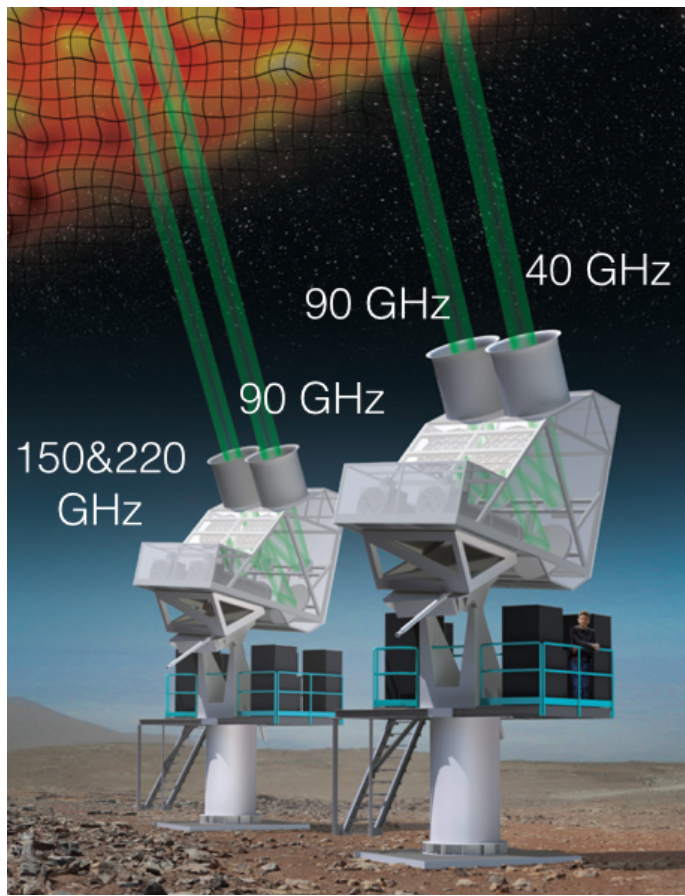


Figure 6: Top: An artist's impression of what the CLASS telescope will look like once deployed in the Atacama Desert, Chile. On the telescope to the right stands a professor, or maybe the ever eternal Fletcher Boone for scale. Disclaimer: The CLASS telescope will not shoot out green laser beams that will melt the sky into an orange and yellow glow. Bottom: The four detection bands of class (shaded in blue) are chosen to avoid atmospheric emission from  $O_2$  and  $H_2O$  [8][9].

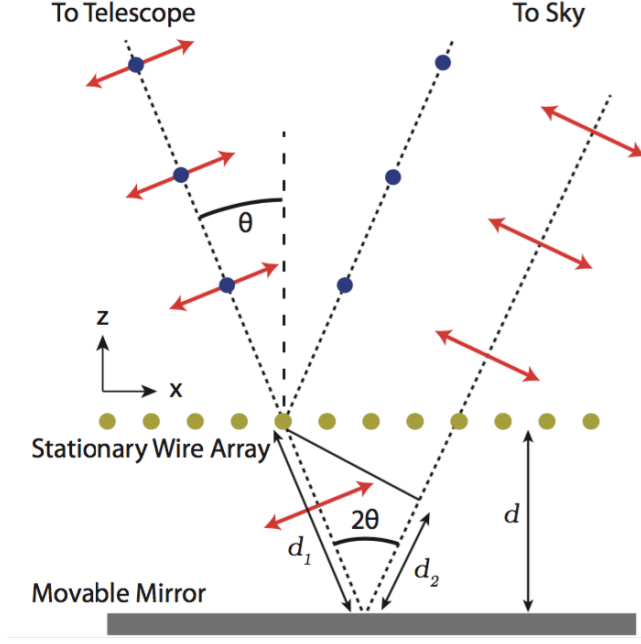


Figure 7: Polarized light is separated and then recombined, creating a phase difference dependent on how far the mirror is from the wire grid (gold dots) [7].

### 5.3 Cryostat

CLASS uses transition-edge-sensor (TES) bolometers to detect the signal from the sky. The signal is then read out and amplified by a series of superconducting quantum interference devices (SQUIDS). This entire setup is housed within one of the four cryostats that CLASS has purchased from BlueFors Cryogenics, and each cryostat will cool the TES bolometers to  $70 \text{ mK}$  using a dilution refrigerator.<sup>6</sup> The main reason why the setup has to be cooled is to reduce photon noise from the optics and phonon noise from the bolometers themselves. Bolometer phonon noise is proportional to the superconducting transition temperature for a TES. Since CLASS detectors have a superconducting transition temperature of around  $150 \text{ mK}$  (made possible because we employ a dilution refrigerator), our detectors will have approximately 50% lower detector noise as opposed to other absorption-fridge systems, which are limited to a superconducting transition temperature of  $500 \text{ mK}$ . In the following sections, the functionality and theory of the components of the cryostat will be explained.

---

<sup>6</sup>BlueFors Cryogenics, Arinatie 10, 00370 Helsinki, Finland, [www.bluefors.com](http://www.bluefors.com)

### 5.3.1 Overall Design

Each cryostat has four cold stages at  $60\text{ K}$ ,  $4\text{ K}$ ,  $1\text{ K}$ , and  $70\text{ mK}$ . The system is cooled first by a pulse tube, and then when the system reaches  $4\text{ K}$ , the dilution refrigerator is turned on to cool the final stages to  $1\text{ K}$  and  $70\text{ mK}$ . The entire system is encased in vacuum sealed cans, so that the system can be brought to a pressure of  $< 1 \times 10^{-3}\text{ mbar}$ . The system is operated in a vacuum in order to reduce ambient heating from gas particles and to reduce unwanted thermal conductivity between stages. Additionally, once the system cools below  $77\text{ K}$ , nitrogen condenses onto the system components which can alter their effectiveness.

Because there is no air in between each stage, the main source of thermal conductivity are heat switches that double as supports connecting the  $4\text{ K}$  stage to the  $1\text{ K}$  and the  $70\text{ mK}$  stage. The heat switches consist of a stainless steel tube that has poor thermal conductivity and two copper heat exchanger parts on each end of the tube. The switches are filled with helium gas, which acts as a thermal conductor. At the end of each heat switch is an outlet that connects to an active carbon pump which activates when the temperature is approximately  $10\text{ K}$ , absorbing all the helium inside the switch. This effectively cuts off the colder stages from the warmer stages since the only way to conduct heat between stages is left to the stainless steel tube with poor thermal conductivity. The heat switches can be turned back on to warm up the cryostat by using small heaters which release the helium from the active carbon pumps. See Figure 8 for a view of some of the cryostat components.

Each cold stage is also isolated from one another by concentric cans that fit over one another like a Matroyoshka doll (aka Russian dolls). The cans are wrapped in blankets of Multi-layer Insulation (MLI) to reduce thermal loading from outside radiation, including blackbody radiation from warmer stages of the cryostat. MLI is comprised of layers of aluminized mylar separated by an insulating mesh known as "wedding veil". Due to blackbody properties, radiation absorbed by the outermost layer will be re-emitted from both sides of the mylar but at half the power of the incident rays. With ten layers of MLI, the power from incoming radiation is effectively reduced by a factor of  $1/2^{10}$  or  $1/1024$ . The "wedding veil" is critical since it prevents the mylar layers from thermally shorting, which would effectively combine two mylar layers into one, reducing the effectiveness of the MLI by a factor of  $1/2$ . In CLASS's cryostats, there are 30 layers of MLI on the can attached to the  $60\text{ K}$  stage and 10 layers of MLI on the can attached to the  $4\text{ K}$  stage. Additionally, because components of CLASS such as the SQUIDs are very sensitive to magnetic fields, the  $4\text{ K}$  can is equipped with magnetic shielding to prevent sources such as the Earth's own magnetic field from affecting the instrument performance.

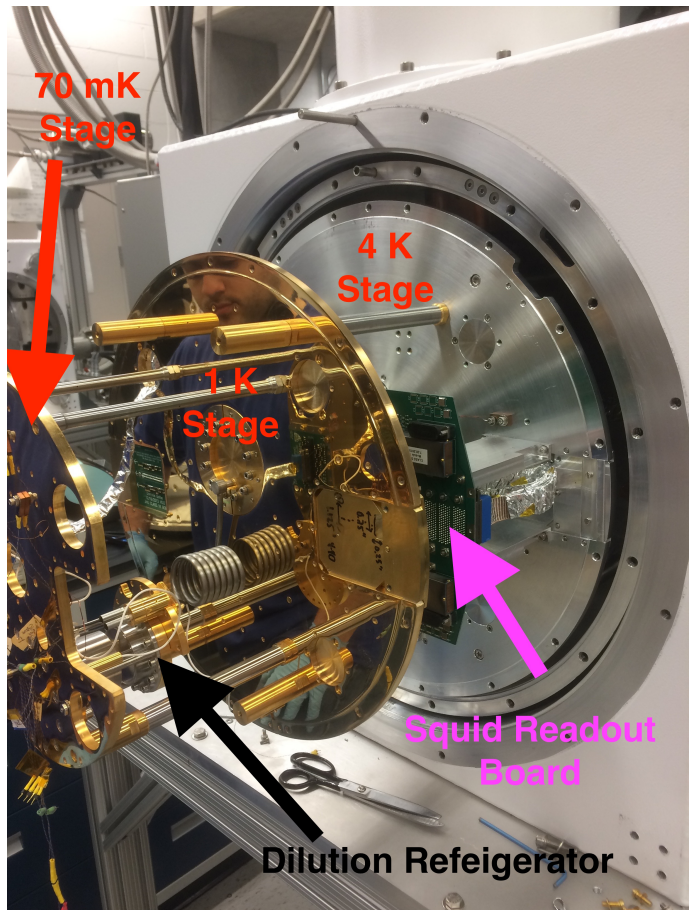


Figure 8: Here is the cryostat opened up and warm. The cryostat must be opened when working on the inner components. Each cold stage consists of a flange, indicated in red, and a corresponding covering can (not shown). The dilution refrigerator is indicated in black, and the SQUID readout board is indicated in purple.

### 5.3.2 Pulse Tube

The Pulse Tube is used to cool the  $60\text{ K}$  and  $4\text{ K}$  stages. Pulse tube refrigerators work through a cyclic compression and expansion of helium gas. The fundamental components of the refrigerators are a pulse tube (which has an open end and a closed end), a regenerator<sup>7</sup>, a pressure wave generator (like a piston), and two heat exchangers (one hot and one cold). To start the cycle, the piston compresses the gas towards the closed end of the pulse tube, causing the temperature of the gas to rise since it is undergoing adiabatic compression. The regenerator also absorbs some heat from the gas. At the closed end of the pulse tube, heat is conducted by the heat exchanger and the temperature of the gas falls. The piston then retracts and the gas cools more as it adiabatically expands. This cools the heat exchanger at the open end of the pulse tube, which is the process that cools down the cryostat. The gas also cools the regenerator, allowing the next cycle to start at a lower temperature than the previous cycle. More information can be found in [4].

### 5.3.3 Dilution Refrigerator

In order to reach the desired temperature of  $70\text{ mK}$ , a dilution refrigerator (DR) must be used. At  $100\text{ mK}$  the DR provides a whopping  $50\text{ }\mu\text{W}$  of cooling power! The dilution refrigerator works with liquid helium, so the system must be cooled to  $< 4.2\text{ K}$  by the pulse tube before the DR is turned on.

The operation principle of a DR depends on the property of a  $3\text{-He}/4\text{-He}$  mixture at low temperatures. At  $2.17\text{ K}$ ,  $4\text{-He}$  turns into a superfluid. When diluted with  $3\text{-He}$ , the mixture possesses the property that at temperatures below  $0.8\text{ K}$ , the mixture will separate into two phases—a pure  $3\text{-He}$  phase and a heavily concentrated  $4\text{-He}$  phase. As the temperature approaches  $0\text{ K}$ , one phase will be  $100\%$   $3\text{-He}$  while the other will be mostly  $4\text{-He}$  with  $6.4\%$  of  $3\text{-He}$ . The reason why the  $4\text{-He}$  phase is diluted with  $3\text{-He}$  is that He is a noble gas, so the main force of interaction between atoms is the Van Der Waals Force. Because the Van Der Waals interaction between  $4\text{-He}$  and  $3\text{-He}$  is stronger than the interaction between two  $3\text{-He}$  atoms, some of the  $3\text{-He}$  atoms diffuse into the  $4\text{-He}$  concentrated phase. Due to the entropy of mixing, the  $4\text{-He}/3\text{-He}$  phase has a higher entropy than the  $3\text{-He}$  pure phase. By pushing atoms from the  $3\text{-He}$  phase to the  $4\text{-He}/3\text{-He}$  phase, the atoms gain entropy and therefore heat, which cools the surroundings and gives the desired refrigeration.

The way the DR works in the BlueFors cryostat is as follows: The pulse tube cools the DR to  $4.2\text{ K}$

---

<sup>7</sup>A regenerator is a heat exchanger with high heat capacity where heat from a hot fluid can be stored before being transferred to a cooler fluid.

allowing the DR cycle to start. The 3-He/4-He mixture is then condensed into the system with the help of cooling and compressors, which raise the pressure to 2 bar. Once condensed, the mixture fills up the mixing chamber (where cooling occurs), the condensing line, the heat exchanger, and part of the still. See Figure 9 for an illustration. The still is then pumped which results in evaporative cooling, bringing the temperature to  $<0.8\text{ K}$  when the phase separation occurs. At this temperature, the 4-He/3-He mixture settles at the bottom since it is heavier than the 3-He pure phase. In the still, which is still being pumped, the helium being evaporated is mostly 3-He because it has a higher vapor pressure than 4-He. The process lowers the concentration of 3-He in the mixture, inducing an osmotic effect where 3-He atoms from the pure phase move into the mixed phase, and as stated before, this process produces the desired cooling effect [5].

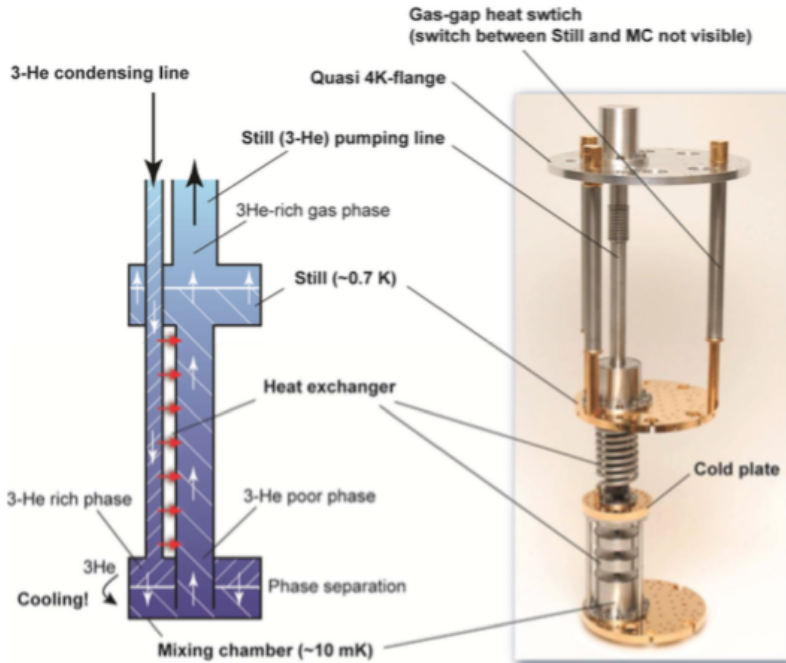


Figure 3. Dilution refrigerator principal parts.

Figure 9: The left is a schematic of the DR, and the right is what the DR actually looks like [5].

### 5.3.4 Thermometry

In order to verify the performance of the the cryostat and diagnose problem areas, CLASS is equipped with two types of thermometers. Silicon diode thermometers are mounted on the 300 K, 60 K, and 4 K stages and cans. Diode thermometers consist of a p-n junction and when a bias current is applied,

the voltage across the junction is inversely proportional to the temperature. The accuracy of the diode thermometers are  $\pm 22 \text{ mK}$  at  $60 \text{ K}$  and  $\pm 12 \text{ mK}$  at  $4 \text{ K}$  [18]. The temperatures on the  $1 \text{ K}$  and  $0.1 \text{ K}$  stages are measured with ruthenium oxide thermometers because they perform better at lower temperatures than the silicon diode thermometers. At  $0.1 \text{ K}$ , the Lake Shore ruthenium oxide thermometers have an accuracy of  $\pm 5 \text{ mK}$  [16]. Also, as opposed to the diode thermometers, they are resistors and not diodes.

The diode thermometers are read out by a CLASS diode readout board which biases the thermometers as well as converts the digital signal from them. The ruthenium oxide thermometers are read out and biased by a Stanford Research Systems Lakeshore 370 GPIB 12 (SRS). Warm multiplexing<sup>8</sup> is useful because it allows the thermometers to be read by one resistance bridge, which is both expensive and bulky. To read more about the wires that run inside the cryostat for the thermometry and detectors, refer to Appendix B.

During cooldowns, the thermometers are used to ensure the desired temperatures are reached and are also useful in diagnosing issues with the cryostat. The temperatures of the thermometers as well as the location of each one give valuable insight into what parts of the cryostat are not cooling as they are supposed to. For example, if different temperature stages of the cryostat are in thermal contact, the thermometer data should reveal this to us. This is especially important because when the cryostat is cooled, the structure of the inside may change producing a touch between stages that we will not see when the cryostat is warm. For example if the can attached to the  $60 \text{ K}$  stage comes into thermal contact with the can attached to the  $4 \text{ K}$  stage, the thermometers associated with the  $4 \text{ K}$  stage may read higher temperatures such as  $8 \text{ K}$  and  $10 \text{ K}$ . The points where the cans touch can be narrowed down by following the thermometers since the  $10 \text{ K}$  one will be closer to the touch than the  $8 \text{ K}$  one. Temperature data from a cooldown can be seen in Figure 10. To read more about the steps when performing a cooldown refer to Appendix C.

### 5.3.5 Detectors

Besides the thermometry, the other important set of electronics within the cryostat are the detectors. CLASS uses feedhorn-coupled transition-edge sensors (TES) bolometers, which are then read out by superconducting quantum interference devices (SQUIDS). The polarization of the incoming light is determined by two orthogonal antennae in the detectors. The readouts are then amplified by a SQUID series array. The readouts are sent to a warm Multi-Channel Electronics (MCE) device which performs the multiplexing. Unlike the warm multiplexing used with the SRS thermometry system, this cold multiplexed system is used to reduce the number of wires going from the cold stages to room temperature, reducing the thermal load

---

<sup>8</sup>Multiplexing is the process of reading one thermometer channel at a time

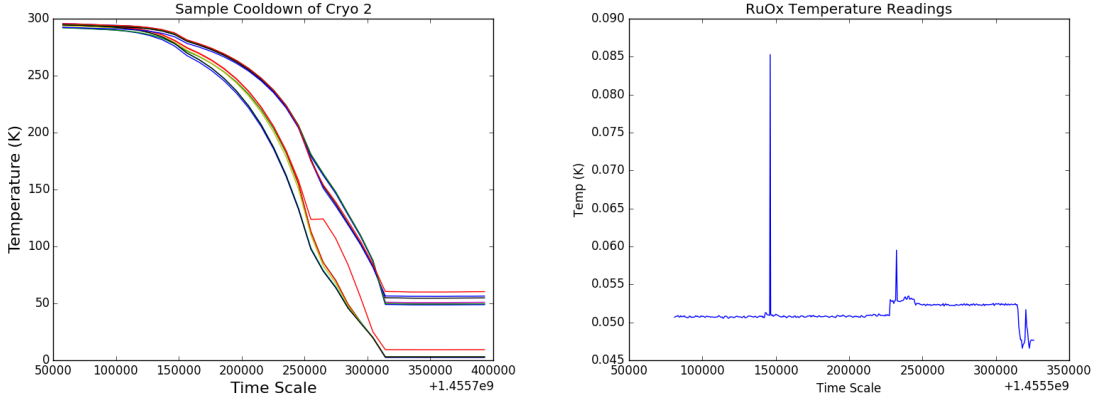


Figure 10: On the left is data from the diodes during a cooldown with each color associated with a different diode. One can see the distinction between thermometers on the  $60\text{ K}$  stage and the  $4\text{ K}$  stage. The temperatures begin to drop when the pulse tube is turned on and plateau when the desired temperatures are reached. When temperatures reach  $77\text{ K}$  one would expect the temperature to drop faster because heat capacities of metals drop significantly below this temperature, but this was not evident during this cooldown. On the right is data from the ruthenium oxide thermometers. The cooldown was not captured by this data set. The resulting temperatures are also calculated by using a calibration curve from Lakeshore converting measured resistances to temperatures. However, each ruthenium oxide thermometer has slightly different calibration curves, so the data shown should be taken with a grain of salt. The data spikes are also extraneous data points given by the SRS.

created by the wires and decluttering the inside of the cryostat.

### TES bolometers

TES bolometers work by operating at the transition temperature of the superconducting phase transition. As a superconductor, materials have no electrical resistance. At the superconducting transition temperature, a small change in temperature results in a substantial change in resistance. By biasing the TES with a voltage, a change in resistance will induce a change in current producing a magnetic field, which is then measured by SQUIDs. The TES is also coupled to a thermal bath into which it can dissipate the heat accumulated by the incoming photons.

The TES bolometers of CLASS are molybdenum-gold superconducting bilayers mounted on silicon wafers and operate at  $150\text{ mK}$ . This temperature is reached by use of heaters since we do not have control over the cooling power of the DR. The DR cools the focal plane where the detectors are located to  $70\text{ mK}$ . Then the TESs self-heat through the joule power law<sup>9</sup> reaching their operating temperature which is also

---

<sup>9</sup>Joule Power Law:  $P_J = \frac{V_{bias}^2}{R_{TES}}$

the superconducting transition temperature.

## SQUIDs

CLASS utilizes DC niobium SQUIDs which consist of a superconducting loop containing two Josephson junctions in parallel. A Josephson junction is two superconductors separated by some non-superconducting layer. In 1962, Brian Josephson postulated that superconducting cooper pairs<sup>10</sup> could tunnel through the non-superconducting layer. The voltage through a Josephson junction is given by

$$U = \frac{\hbar}{2e} \frac{\partial\phi}{\partial t}$$

where  $U$  is the voltage,  $\hbar$  is Planck's constant,  $e$  is the electric charge, and  $\phi$  is the phase difference across the junction. The current in a Josephson junction is governed by the equation:

$$I = I_c \sin\phi$$

where  $I_c$  is the critical current of the junction (the maximum current the junction will allow). At a current  $I > I_c$ , the junction acts as a resistor and a voltage appears across the junction.

A DC SQUID uses the fact that magnetic fluxes are quantized. The value of a magnetic flux is

$$\Phi_0 = \frac{2\pi\hbar}{2e} = 1.0678 \times 10^{-15} Tesla \cdot m^2$$

When a magnetic flux enters the SQUID it induces a screening current through Lenz's Law. The screening current adjusts itself so that the total flux through the SQUID is a multiple of the magnetic flux. For example, a magnetic flux between  $n \cdot \Phi_0$  and  $\Phi_0(n + 1/2)$  (where  $n$  is an integer), will induce a current that opposes the magnetic flux so that the total flux is equal to  $n \cdot \Phi_0$ . For a flux between  $\Phi_0(n + 1/2)$  and  $\Phi_0(n + 1)$ , the induced current will increase the total flux to equal  $\Phi_0(n + 1)$ . In the first case, the induced current opposes the flux, while in the second case the induced current contributes to the flux. This means that the current switches direction around the SQUID loop every time the original flux through the loop is equal to  $n \cdot \Phi_0/2$ . Essentially, the induced current oscillates sinusoidally as the flux through the SQUID is increased/decreased. If the SQUID is biased by a current  $I > I_c$  and the Josephson junctions act as resistors, then a voltage can be measured across the SQUID that also oscillates sinusoidally with a period equal to

---

<sup>10</sup>Cooper pairs are described by BCS superconducting theory. They are essentially two electrons that are bound together forming a boson. They appear when a material becomes superconducting.

one magnetic quantum flux. A schematic of a DC SQUID is shown in Figure 11.

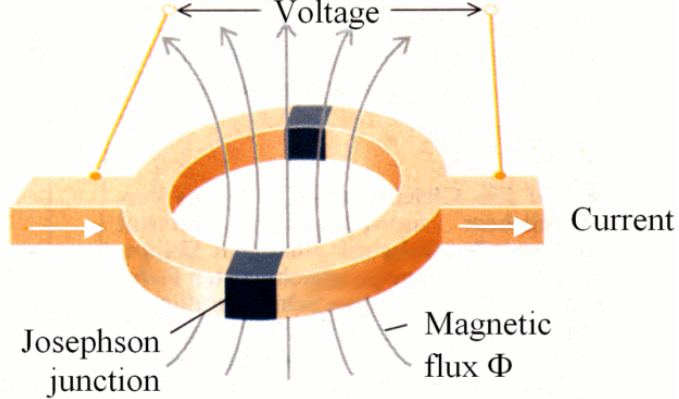


Figure 11: A DC SQUID showing a magnetic flux enclosed by the Josephson junctions in parallel [19].

In CLASS, the SQUIDs are coupled to the TES receivers through an inductor. An inductor in the TES circuit produces a magnetic field when a photon hits the TES. The magnetic field is then read out by a SQUID array. The SQUID array is a bunch of SQUIDS in series all biased above their critical current and reading the same flux. By connecting them in this way the voltage drop across them is amplified, thus amplifying the signal from the TES.

In order to gather the most sensitive readings, the flux through the SQUIDs must be kept at a value where the voltage per change in flux is greatest. This is achieved by coupling the SQUIDs to a feedback loop that induces a magnetic field through the SQUID to counteract the induced field from the TES inductor, keeping the magnetic flux at a value that makes the SQUID the most sensitive. The amount of current needed to induce the field from the feedback loop can then be measured. From this measurement, the field generated by the photon hitting the TES receiver can then be deduced. Calibration curves for the SQUID arrays is shown in Figure 12.

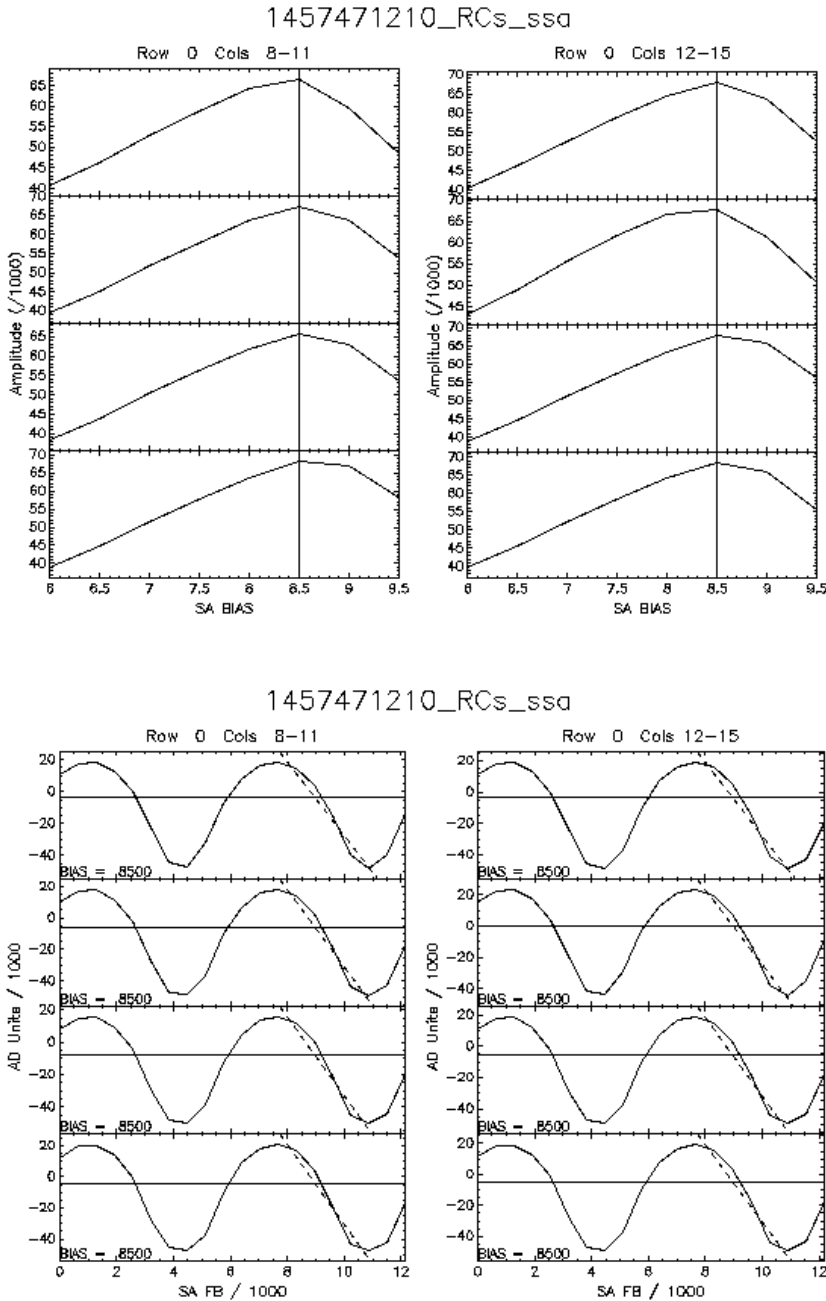


Figure 12: The SQUIDs were first calibrated to determine the bias at which they should be operated. Top: Shows a cycling of different bias values on the x-axis and the amplitude of the sinusoidal voltage curves on the y-axis. The vertical line on each curve indicates the bias at which the amplitude is greatest, meaning the curve will be most sensitive. Bottom: We cycle through different feedback fluxes (x-axis) and display the voltage on the y-axis. The sinusoidal dependence on the flux can be seen, and the dotted line depicts where the slope of the curve is the greatest. This demarcates the flux at which we desire to run through the SQUID to keep it at its most sensitive. The values along the axis in each graph are given in DAC units which can be converted to the units detailed above.

## 6 Conclusion

During the course of the year, we were able to cool down the cryostat to  $25\text{ mK}$  and install the necessary thermometry and detector wiring. The next step includes installing the detectors into the cryostat and preparing the cryostat for shipment down to Chile. In the near future, we hope to have all four cryostats in the field collecting data on the CMB.

# Appendices

## Appendix A The Cosmological Equations

This section will introduce the math behind the dynamics and evolution of our universe for a more comprehensive description. All the mathematics assumes that the distribution of matter in the universe is isotropic and homogeneous on scales larger than 300 *Mpc*.<sup>11</sup> This assumption is known as the Cosmological Principle and means our equations will not define the behavior of singular planets and galaxies but rather the overall evolution of the universe. To describe distances in our universe we use the Robertson-Walker metric:

$$ds^2 = -c^2 dt^2 + a(t)^2 [dr^2 + S_\kappa(r)^2 d\Omega^2] \quad (1)$$

where  $a(t)$  is the scale factor that relates how distances expand or contract with time and  $S_\kappa(r)$  is defined as:

$$S_\kappa(r) = \begin{cases} R\sin(r/R) & (\kappa = +1) \\ r & (\kappa = 0) \\ R\sinh(r/R) & (\kappa = -1) \end{cases}$$

These cases describe the curvature of the universe where  $R$  is the radius of curvature,  $r$  is a distance, and  $\kappa$  describes the type of curvature. For  $\kappa = +1$ , the universe is positively curved like a sphere; for  $\kappa = 0$ , it is flat like a plane; and for  $\kappa = -1$ , it is negatively curved like a saddle.

Once Einstein published the theory of general relativity in 1915, which linked the curvature of space-time with the mass-energy content of the universe, Alexander Friedmann was able to develop his equations to govern the expansion of space in a homogeneous and isotropic universe. The following equation relates the evolution of the scale factor  $a(t)$  to the pressure and energy of the universe.

$$\left(\frac{\dot{a}}{a}\right)^2 = \frac{8\pi G}{3c^2} \epsilon(t) - \frac{\kappa c^2}{R_0^2} \frac{1}{a(t)^2}$$

Here  $\epsilon(t)$  is the energy density of the universe,  $G$  is the universal gravitational constant, and  $R_0$  is

---

<sup>11</sup>Isotropy is the notion that the distribution of matter is the same no matter in what direction you look, and homogeneity is the notion that the distribution of matter is the same no matter where in the universe you are.

the radius of curvature of the universe at present day. By defining the Hubble Parameter,  $H(t) \equiv \dot{a}/a$  and the Hubble Constant  $H_o = H(t_0)$ , where

$$H(t_0) = \left( \frac{\dot{a}}{a} \right)_{t=t_0}$$

we can rewrite the Friedmann equation as

$$H(t)^2 = \frac{8\pi G}{3c^2} \epsilon(t) - \frac{\kappa c^2}{R_0^2 a(t)^2}.$$

Now for a spatially flat universe where ( $\kappa = 0$ ), the Friedmann equations takes the form:

$$H(t)^2 = \frac{8\pi G}{3c^2} \epsilon(t).$$

For a given Hubble parameter, one can solve for  $\epsilon(t)$ , which then becomes the critical density that will determine a flat universe [17]:

$$\epsilon_c(t) \equiv \frac{3c^2}{8\pi G} H(t)^2.$$

From this we can define the energy density parameter  $\Omega$  in section 3.2.1 as:

$$\Omega(t) = \frac{\epsilon(t)}{\epsilon_c(t)}.$$

## Appendix B TekData Cables

We use TekData cables to read our thermometers and detectors. They carry the signal and bias lines to the warm electronics. These cables are manganin cables with MDM connectors. The wires are a twisted pair to prevent pick up, and they are wound with aramid fiber for durability. The MDM connectors are also strain relieved with low-profile epoxy black shells [2]. We use these wires because they have low thermal conductivity, which is critical given the cables are in thermal contact with each temperature stage of the cryostat. The wires are then wrapped with mylar to prevent electromagnetic interference. Since the wires are carrying current, they produce a magnetic field which we do not want interfering with the signals in other cables. It also shields the cables from external radiation. The external radiation may come from leakages in the cans or the other electronics within the cryostat. The mylar shielding is also wrapped by bare manganin wire to ground any charge that collects on the shielding. We need to use bare (uncovered)

manganin wire so it is in electrical contact with the shielding itself, allowing excess charge to flow from the mylar to ground. The wire is grounded by attaching it to a copper tab which is then attached to one of the cryostat's flanges.

Both the thermometers and detector cables are separated on each side of the cryostat. Thermometers were placed on each flange of the cryostat and along their respective cans. This helps us understand how the cryostat is cooling. For example, if there is a touch (when cans from different temperature stages are in direct thermal contact), the thermometers along the cans will be warmer or colder than the thermometers on the flanges depending on what stages are in contact. The thermometers are then connected to circuit boards on the flanges, and the signal is carried out of the cryostat through the TekData cables. The idea is the same as the detector wiring, except all the wires go to the squid readout board between the 4  $K$  and 1  $K$  stages.

## Appendix C Cryostat Operating Procedures

The following procedure was used when only the thermometry was installed. Below is the list of items to make sure are completed before starting to cool the cryostat.

### C.1 These are activities that should only have to be done once

- Wrap the cans in MLI<sup>12</sup>: The radiation shields (we shall refer to them as cans) from BlueFors were not sufficiently wrapped since the layers were not wrapped layer by layer. BlueFors put a 10 layered sheet on top of another 10 layered sheet at the seam effectively putting the top layer and bottom layer in contact. Each layer should only be in contact with itself and insulated by the wedding veil on either side. Additionally, the 60  $K$  stage needs 30 layers, so that includes the can and the short can.
- Wrap backside of 60 K flange with MLI. Make sure not to tape the interface that will be used when attaching the 60 K can to the flange.
- Wrap and ground TekData<sup>13</sup> cables: Wrapping the TekData cables with Mylar and grounding them with manganin thin uninsulated wire protects the cables from electromagnetic waves . We use manganin because it is electrically conductive but not thermally conductive. This is important because the wire

---

<sup>12</sup>MLI is an acronym for multi-layered insulation. We use Mylar to reflect radiation with a wedding veil insulation between each sheet of Mylar to insulate the sheets from each other.

<sup>13</sup>TekData cables are specialized cables woven into fabric for strength and which connect our thermometers and detectors to their respective readout electronics.

is connected to different temperature stages and we do not want extra thermal conductivity between two stages.

## C.2 These are activities that should be checked every time the cryostats are closed

- Make sure all holes in the flanges are plugged including the spaces where the thermometry and detector circuit boards are placed: We do not want extra thermal loading from photons that can reach the cooler stages from the warmer stages.
- Clean all surfaces where the cans will connect to the flanges: Materials such as adhesive residue from tape will reduce the conductivity between the flanges and the cans. Other materials may also prevent the cans and flanges from becoming flush with each other and a small bump will prevent the cans and flanges from being in good contact.
- Check which thermometer is associated with which read-out channel: (The location of each thermometer, especially the ones along the can and at the end of the can should be noted. This helps when determining where extra heat loading is occurring when 'debugging' the cryostat. This activity is done manually by reading each channel and unplugging each thermometer to determine which channel corresponds to which thermometer.)

The following are the procedures to cool the cryostat once the checks have been completed.

1. Make sure all checks listed above have been completed.
2. Attach short can. For all can attachments below make sure to clean (with isopropanol) the surface of the can that will be in contact with the flange. Make sure there is no space between the flange and the cans once the bolts have been tightened. The bolts should be tightened as much as possible with a screwdriver–no Allen wrench needed. Additionally, when adding each can it is helpful to remove the tops of the cans to see if one stage is in contact with another (a touch), reducing the effectiveness of cooling.
3. Attach copper can to 1  $K$  stage.
4. Attach 4  $K$  can and make sure relevant wires are accessible to be plugged in. (This is the trickiest can to align on cryo 2. A good method is to have one person maneuver the can into a position where the

can is flush with the flange while someone else is ready to screw in the top bolts. The bolting person can also have the bolts halfway in while person one is maneuvering the can.)

5. Attach 60k can.
6. Attach vacuum can. Make sure o-rings and o-ring surfaces are clean. Metal interfaces can be cleaned with isopropanol and rings can be cleaned by rubbing them with gloved hands. Do not clean rings with isopropanol and make sure all isopropanol has evaporated before putting ring on can since rings can absorb isopropanol which is detrimental when trying to create a vacuum as isopropanol will be slowly leaked out.
7. **MAKE SURE THERE IS NO HELIUM MIXTURE IN THE DR SYSTEM. PUMP IT ALL BACK INTO THE MIXTURE TANK!**
8. Start pumping on the vacuum tank with the roughing pump.
9. Leak check the system with helium. Using a mass spectrometer to detect helium, spray helium along all crevices of the cryostat system starting at the top and moving down (helium rises so starting at the bottom may cause the spectrometer to react even though the leak is above the area being sprayed.) Make sure to check all vacuum can connections as well as side panels and valves, even if not used, on the backside of the cryostat box. The mass spectrometer should be attached to the vacuum pump, which is evacuating air from the system so any helium that leaks into the system will be detected.
10. Once pressure reaches less than 1 millibar, turbopumps can be started.
11. When the pressure of the vacuum can is  $< 1 \times 10^{-3} \text{ mbar}$  (p1) the pulse tube can be started.
12. When the temperature of the 4 K flange reaches 4 K, the DR can be started.

## Appendix D Site Work

### D.1 Acquiring Data

Through the command execution interface one can run:

```
MCEQ -autosetup  
MCEQ -autobias
```

Where -autosetup, sets up the SQUID readout, and should always be run before autoiv, because it resets the detector biases to zero every time. -autoiv (I think is the same as -autobias), acquires an I-V curve by sweeping the detector bias, it then analyses the results, chooses the optimal bias for each column and sets that bias. At this point the detectors are on and we can acquire data. After running -autobias, it is wise to wait a minute because the -autobias command sends a voltage through the detectors, heating them up. After waiting a minute we can then run

```
MCEQ -acqdata 25000
```

The number after -acqdata indicates how many data points to take. CLASS samples at 200 samples per second so in this case 25000 would indicate taking data for 125 seconds.

## References

- [1] URL: <http://abyss.uoregon.edu/~js/cosmo/lectures/lec15.html> (visited on 05/04/2016).
- [2] John W. Appel, Aamir Ali, Mandana Amiri, Derek Araujo, Charles L. Bennett, Fletcher Boone, Manwei Chan, Hsiao-Mei Chod, David T. Chuss, Felipe Colazo, Erik Crowe, Kevin Denis, Rolando Dünner, Joseph Eimer, Thomas Essinger-Hileman, Dominik Gothe, Mark Halpern, Kathleen Harrington, Gene Hilton, Gary F. Hinshaw, Caroline Huang, Kent Irwin, Glenn Jones, John Karakla, Alan J. Kogut, David Larson, Michele Limon, Lindsay Lowry, Tobias Marriage, Nicholas Mehrle, Amber D. Miller, Nathan Miller, Samuel H. Moseley, Giles Novak, Carl Reintsema, Karwan Rostema, Thomas Stevenson, Deborah Towner, Kongpop U-Yen, Emily Wagner, Duncan Watts, Edward Wollack, Zhilei Xu, and Lingzhen Zeng. “The Cosmology Large Angular Scale Surveyor (CLASS): 38 GHz detector array of bolometric polarimeters”. In: *Millimeter, Submillimeter, and Far-Infrared Detectors and Instrumentation for Astronomy VII* 9153, 9153J (2014). DOI: [10.1117/12.2056530](https://doi.org/10.1117/12.2056530).
- [3] Neta Bahcall, Jeremiah Ostriker, Saul Perlmutter, and Paul Steinhardt. “A Cosmic Triangle: Assessing the State of the Universe”. In: *Science* 284:1481-1488, 1999 (2008). DOI: [10.1126/science.284.5419.1481](https://doi.org/10.1126/science.284.5419.1481).
- [4] J. Bert. *Pulse Tube Cryocoolers: A Cogen-Free Path to 2K*. 2007. URL: <http://large.stanford.edu/courses/2007/ph210/bert2/> (visited on 05/26/2016).
- [5] “BF-LD400 Cryogen-Free Dilution Refrigerator System User Manual”. In: (2013).
- [6] Sarah Church. URL: [http://web.stanford.edu/~schurch/quad\\_science.html](http://web.stanford.edu/~schurch/quad_science.html) (visited on 05/04/2016).
- [7] Joseph R Eimer. “The Cosmology Large Angular Scare Surveyor (CLASS): In Search of the Energy Scale of Inflation”. In: (2013).
- [8] Thomas Essinger-Hileman, Mandana Amiri Aamir Ali, John W. Appel, Derek Araujo, Charles L. Bennett, Fletcher Boone, Manwei Chan, Hsiao-Mei Cho, David T. Chuss, Felipe Colazo, Erik Crowe, Kevin Denis, Rolando Dünner, Joseph Eimer, Dominik Gothe, Mark Halpern, Kathleen Harrington, Gene Hilton, Gary F. Hinshaw, Caroline Huang, Kent Irwin, Glenn Jones, John Karakla, Alan J. Kogut, David Larson, Michele Limon, Lindsay Lowry, Tobias Marriage, Nicholas Mehrle, Amber D. Miller, Nathan Miller, Samuel H. Moseley, Giles Novak, Carl Reintsema, Karwan Rostem, Thomas Stevenson

- Stevenson, Deborah Towner, Kongpop U-Yen, Emily Wagner, Duncan Watts, Edward Wollack, Zhilei Xu, and Lingzhen Zeng. In: (2014). DOI: [10.1117/12.2056701](https://doi.org/10.1117/12.2056701).
- [9] Kathleen Harrington, Tobias Marriage, Aamir Ali, John W. Appel, Charles L. Bennett, Fletcher Boone, Michael Brewer, Manwei Chan, David T. Chuss, Felipe Colazo, Sumit Dahal, Kevin Denis, Rolando Dünner, Joseph Eimer, Thomas Essinger-Hileman, Pedro Fluxa, Mark Halpern, Gene Hilton, Gary F. Hinshaw, Johannes Hubmayr, Jeffery Iuliano, John Karakla, Jeff McMahon, Nathan T. Miller, Samuel H. Moseley, Gonzalo Palma, Lucas Parker, Matthew Petroff, Bastián Pradenas, Karwan Rostem, Marco Sagliocca, Deniz Valle, Duncan Watts, Edward Wollack, Zhilei Xu, and Lingzhen Zengh. “The Cosmology Large Angular Scale Surveyor”. In: *Proc. SPIE 9914, Millimeter, Submillimeter, and Far-Infrared Detectors and Instrumentation for Astronomy VIII, 99141K* (19 July 2016); 9914, 99141K (2016). DOI: [10.1117/12.2233125](https://doi.org/10.1117/12.2233125).
- [10] G. Hinshaw, D. Larson, E. Komatsu, D. N. Spergel, C. L. Bennett, J. Dunkley, M. R. Nolta, M. Halpern, R. S. Hill, N. Odegard, L. Page, K. M. Smith, J. L. Weiland, B. Gold, N. Jarosik, A. Kogut, M. Limon, S. S. Meyer, G. S. Tucker, E. Wollack, and E. L. Wright. “Nine-Year Wilkinson Microwave Anisotropy Probe (WMAP) Observations: Cosmological Parameter Results”. In: *ArXive* (2012). DOI: [10.1088/0067-0049/208/2/19](https://doi.org/10.1088/0067-0049/208/2/19).
- [11] Wayne Hu and Martin White. “A CMB Polarization Primer”. In: *New Astron* 2:323 (1997). DOI: [10.1016/S1384-1076\(97\)00022-5](https://doi.org/10.1016/S1384-1076(97)00022-5).
- [12] Lindsay Ng Lowry. “Testing and Optimization Analysis of the CLASS Variable-Delay Polarization Modulators”. In: (2013).
- [13] *Polarized Emission From Milky Way Dust*. 2015. URL: [http://www.esa.int/spaceinimages/Images/2015/02/Polarised\\_emission\\_from\\_Milky\\_Way\\_dust](http://www.esa.int/spaceinimages/Images/2015/02/Polarised_emission_from_Milky_Way_dust) (visited on 06/07/2017).
- [14] Adam G. Riess, Alexei V. Filippenko, Peter Challis, Alejandro Clocchiattia, Alan Diercks, Peter M. Garnavich, Ron L. Gilliland, Craig J. Hogan, Saurabh Jha, Robert P. Kirshner, B. Leibundgut, M. M. Phillips, David Reiss, Brian P. Schmidt, Robert A. Schommer, R. Chris Smith, J. Spyromilio, Christopher Stubbs, Nicholas B. Suntzeff, and John Tonry. “Observational Evidence from Supernovae for an Accelerating Universe and a Cosmological Constant”. In: *Astronomical Journal* 116 (1998), pp. 1009–1038. DOI: [10.1086/300499](https://doi.org/10.1086/300499).
- [15] Vera Rubin. “Rotation of the Andromeda Nebula from a Spectroscopic Survey of Emission Regions”. In: *The Astrophysical Journal* 159 (1970), p. 379. DOI: [10.1086/150317](https://doi.org/10.1086/150317).

- [16] *Ruthenium Oxide (Rox)*. 2016. URL: <http://www.lakeshore.com/products/cryogenic-temperature-sensors/ruthenium-oxide-rox-rtds/models/pages/Specifications.aspx> (visited on 05/26/2016).
- [17] Barbara Ryden. *Introduction to Cosmology*. San Francisco, California: Addison Wesley, 2003.
- [18] *Silicon Diodes*. 2016. URL: <http://www.lakeshore.com/products/cryogenic-temperature-sensors/silicon-diodes/dt-670/pages/Specifications.aspx> (visited on 05/26/2016).
- [19] *SQUID*. URL: <http://www.engr.sjsu.edu/rkwok/squid.htm> (visited on 06/07/2017).
- [20] "WMAP "Science on a Sphere" Microwave Sky Images Five Year Maps". 2012. URL: <http://lambda.gsfc.nasa.gov/product/map/dr4/sos/5year/> (visited on 05/05/2016).
- [21] Matias Zaldarriaga. "The Polarization of the Cosmic Microwave Background". In: (2003). DOI: arXiv: astro-ph/0305272.
- [22] Fritz Zwicky. "Die Rotverschiebung von extragalaktischen Nebeln". In: *Helv. Phys. Acta* 6 (1933), pp. 110–127.